

Inverse Reinforcement Learning for Minimum-Exposure Paths in Spatiotemporally Varying Scalar Fields^{*}

Alex Ballentine^{*} Raghvendra V. Cowlagi^{*}

^{*} *Aerospace Engineering Department, Worcester Polytechnic Institute,
Worcester, MA USA 01609 E-mail: aeballentine, rvcowlagi@wpi.edu.*

Abstract: Performance and reliability analyses of autonomous vehicles (AVs) can benefit from tools that “amplify” small datasets to synthesize larger volumes of plausible samples of the AV’s behavior. We consider a specific instance of this data synthesis problem that addresses minimizing the AV’s exposure to adverse environmental conditions during travel to a fixed goal location. The environment is characterized by a threat field, which is a strictly positive scalar field with higher intensities corresponding to hazardous and unfavorable conditions for the AV. We address the problem of synthesizing datasets of minimum exposure paths that resemble a training dataset of such paths. The main contribution of this paper is an inverse reinforcement learning (IRL) model to solve this problem. We consider time-invariant (static) as well as time-varying (dynamic) threat fields. We find that the proposed IRL model provides excellent performance in synthesizing paths from initial conditions not seen in the training dataset, when the threat field is the same as that used for training. Furthermore, we evaluate model performance on unseen threat fields and find low error in that case as well. Finally, we demonstrate the model’s ability to synthesize distinct datasets when trained on different datasets with distinct characteristics.

Keywords: Intelligent Autonomous Vehicles; Computational Intelligence in Control; Modeling, Identification and Signal Processing; Inverse Reinforcement Learning; Machine Learning in modeling, estimation, and control; Unmanned Ground and Aerial Vehicles

1. INTRODUCTION

Performance- and reliability analyses of an autonomous vehicle (AV) require an understanding or “explanation” of the underlying autonomy stack, as well as a large number of samples of the vehicle’s operation (Young et al., 2017). However, such information is difficult to obtain because of high cost of real-world operations and proprietary hardware and software. Due to the widespread use of machine learning in autonomy, an explanation of autonomous behaviors is not always available, even to the manufacturer. More commonly, a high-level description of the autonomy stack and a dataset of a small number of samples of the AV’s operation are available. In this situation, performance- and reliability analyses can benefit on tools that can “amplify” the small dataset to synthesize larger volumes of plausible samples of the AV’s behavior.

Synthesis of a large volume of data that is statistically similar to a given training dataset can be accomplished by a generative machine learning model (Ruthotto and Haber,

2021). Widely used generative models include generative adversarial networks, variational autoencoders, and transformer neural networks. In the present context, however, we seek an explainable model, as well as the ability to incorporate a high-level description of the objectives of the vehicle’s autonomous behavior. To this end, we study inverse reinforcement learning (IRL) for the specific problem of autonomous navigation in unstructured environments.

Related work: Imitation learning, or apprenticeship learning, aims to mimic an expert’s behavior. In imitation learning, the goal may either be to directly learn the policy or to learn a reward function which explains an expert’s actions (Naranjo-Campos et al., 2024). Two main approaches include behavioral cloning (BC), following the direct approach, and IRL, following the indirect approach. BC maps the environmental states to expert actions to decide new actions. However, BC relies on previous demonstrations, making it less effective at responding to novel situations (Zare et al., 2024). IRL aims to solve the challenge of determining an agent’s reward function from a given policy or observed behavior (Arora and Doshi, 2021). Once the algorithm determines the reward function, IRL algorithms use reinforcement learning (RL) to extrapolate the policy from the reward function. IRL agents learn through interacting with the environment and altering their behavior based on the results of their actions (Zare et al., 2024).

^{*} This research was sponsored by the DEVCOM Analysis Center and was accomplished under IDIQ Number W911NF-22-2-0001. The views and conclusions contained in this document are those of the authors and should not be interpreted as representing the official policies, either expressed or implied, of the Army Research Office or the U.S. Government. The U.S. Government is authorized to reproduce and distribute reprints for Government purposes notwithstanding any copyright notation herein.

IRL is most useful in applications where an explicit reward function is either difficult to formulate or unknown, for instance in mimicking human behavior. Additionally, IRL provides a more flexible framework which is capable of adapting in dynamic environments, compared to RL where the reward function is pre-defined and error-prone (Naranjo-Campos et al., 2024). Some applications of IRL include training an agent to play video games (Tucker et al., 2018), modeling human interactions and navigation (Martinez-Gil et al., 2020), and water management (Likmeta et al., 2021). IRL has also been used for path-planning by learning from expert demonstrations. Some examples include training algorithms for self-driving cars (Huang et al., 2023) and modeling navigation through human-centric environments, such as crowds, where the shortest path is less important (Feng et al., 2024).

Ng and Russell (2000) proposed some of the first inverse reinforcement algorithms by formalizing the IRL problem with Markov decision processes. The basis for RL is that the reward function is the most representative definition of a given task. IRL extends this to apprenticeship learning, where the reward function is not known, but there are known expert demonstrations. At the time of their work, they describe some of the primary problems with IRL, including dealing with sub-optimal data and observations, learning "easy" reward functions, partially observable environments, and maximizing the identifiability of the reward function (Ng and Russell, 2000). Ziebart et al. (2008) propose maximum entropy approach to IRL that can provide a convex, computationally efficient problem formulation.

One important challenge of IRL is the ambiguity of any potential solution. IRL has always been an ill-posed problem, i.e., that there are multiple possible reward functions that can describe the behavior of an expert (Cao et al., 2021). Some explored solutions include comparing the value function of the expert with the value function of the learner, in which case the error goes to zero if both policies are equivalent or both are optimal. Another solution includes comparing the state-action pairs of the expert and those of the learner (Arora and Doshi, 2021).

While the exploration inherent in IRL algorithms provides robustness compared to BC, IRL is more computationally expensive to train. Further, IRL algorithms can be unpredictable while training, making them dangerous to train outside of simulation, and have poor sampling efficiency as a typical method involves alternating between updating the reward and training the policy (Zare et al., 2024). Brown and Niekum (2019) propose a method of reducing the requisite number of demonstrations for IRL, called machine teaching, which aims to provide an informative set of demonstrations. This algorithm can partially reduce the computational cost of gathering demonstrations and allows for an IRL algorithm that can learn more efficiently.

We are specifically interested in the application of IRL to discrete optimization problems, a common problem to benchmark IRL algorithms. The literature reports some applications of IRL in small grid-world problems (Dong and Wang, 2024) and tabular problems, such as the Gymnasium environments pendulum and cart-pole (Baimukashiev et al., 2024). Martinez-Gil et al. (2020) propose to

compare the feature expectation functions of the expert with those of the learner to evaluate the chosen reward function. The selection of appropriate feature is very important in both IRL and RL problems. In RL, reward function design has a large impact on the behavior of the agent: a poorly chosen reward function may lead to unpredictable and unwanted behavior (François-Lavet et al., 2018). Similarly, the success of IRL is closely related to the choice of features and accurate descriptions of state transitions (Arora and Doshi, 2021).

Contributions: In this paper, we consider a specific instance of the aforesaid data synthesis problem that addresses minimum exposure to adverse environmental conditions during travel to a fixed goal location. The environment is characterized by a threat field, which is a time-varying strictly positive scalar field with higher intensity regions corresponding to potentially hazardous and unfavorable conditions to the AV. We are interested in policies that minimize the AV’s exposure to threat. Note that the high-level description “minimize exposure to threat” may be interpreted via several slightly different reward functions. Indeed, different blackbox autonomy stacks for AVs that each claim to “minimize exposure to threat” may in fact use slightly different cost functions that are unknown to the user. We address the problem of synthesizing datasets of minimum exposure paths that resemble a training dataset of paths. In this paper, we focus on small datasets where we may quantify similarity of the synthesized dataset to the training datasets by direct error calculations. However, the proposed work is agnostic to the size of datasets and may be extended in the future to larger training and synthetic datasets, where similarity is quantified by statistical analysis.

The main contribution of this paper is an IRL model that solves the aforesaid data synthesis problem. We consider time-invariant (static) as well as time-varying (dynamic) threat fields. We find that the proposed IRL model provides excellent performance for synthesizing paths from initial conditions not seen in the training dataset when the threat field is the same as used for training. Furthermore, we evaluate model performance on unseen threat fields and find low error in that case as well. Finally, we demonstrate the model’s ability to synthesize distinct datasets when trained on different datasets with distinct characteristics.

The rest of this paper is organized as follows. In §2, we provide a precise problem formulation. In §3, we describe the details of the proposed IRL model and its training. In §4, we provide results of computational work regarding the performance of the proposed model, and conclude the paper in §5.

2. PROBLEM FORMULATION

Let \mathbb{R}, \mathbb{N} denote the sets of real and natural numbers, respectively. We denote by $\{N\}$ the set $\{1, 2, \dots, N\}$, and by \mathbf{I}_N the identity matrix of size N , for any $N \in \mathbb{N}$. Finally, $\mathbb{U}(a, b)$ denotes the uniform distribution over the interval $[a, b]$, for $a, b \in \mathbb{R}$ and $a < b$.

Consider a closed square region in \mathbb{R}^2 within which the AV operates, overlaid with a grid consisting of N_G points.

Time is discretized over N_T time steps. The methods proposed in this work do not necessitate uniform discretization, but for the sake of simplicity and clarity of the main ideas, the numerical results are restricted to uniform discretizations in space and time. The AV traverses grid points according to the “4-way adjacency rule,” such that the adjacent points are top, down, left, and right. We assume a constant speed such that the actor’s transitions to adjacent grid points occurs in a constant time step δ_t .

The AV’s motion is thereby modeled by a Markov Decision Process (MDP) $\langle \mathcal{S}, \mathcal{U}, \tau \rangle$. For static environments, $\mathcal{S} \equiv \{N_G\}$ is a finite set of observable states, with each state uniquely associated with the AV’s location at a grid point. For dynamic environments, $\mathcal{S} \equiv \{N_G\} \times N_T$, and each state is uniquely associated with the AV’s location at a grid point at a unique time step. The grid point and/or time step associated with a state s are denoted x_s and t_s , respectively. $\mathcal{U} = \{\uparrow, \downarrow, \leftarrow, \rightarrow\}$ is a set of possible actions that enables transition to another state. $\tau : \mathcal{S} \times \mathcal{U} \times \mathcal{S} \rightarrow \{0, 1\}$ is a *transition function* such that $\tau(s, u, s')$ indicates whether or not state s' can be reached from s under action u . This function is a restrictive form of the more general transition probability distribution typically associated with an MDP. For any $s \in \mathcal{S}$, a *neighbor* state s' is such that there exists an action $u \in \mathcal{U}$ with $\tau(s, u, s') = 1$.

Transitions are characterized by a *reward function* $r : \mathcal{S} \times \mathcal{U} \times \mathcal{S} \rightarrow \mathbb{R}$, which maps a state-action pair to a scalar reward. A *policy* π maps the current state to the next state. It can be either a deterministic function $\pi : \mathcal{S} \rightarrow \mathcal{U}$, or a probability distribution over \mathcal{U} . Each policy is associated with a value function $V^\pi : \mathcal{S} \rightarrow \mathbb{R}$, which is the cumulative expected reward for the policy π for any initial state $s_0 \in \mathcal{S}$, namely:

$$V^\pi(s_0) := \mathbb{E}_{s, \pi(s)} \left[\sum_{k=0}^{\infty} \gamma^k r(s_k, \pi(s_k)) \right],$$

where $\gamma \in (0, 1]$ is a discount factor for future rewards. For policy π , every initial state s_0 is associated with a *path*, namely a sequence of states $\mathbf{s} = (s_0, s_1, \dots, s_k, \dots)$ such that s_k is a neighbor of s_{k-1} for each $k \in \mathbb{N}$. Because we consider deterministic transitions in the MDP, every initial state is *uniquely* associated with a path. In this paper, we focus on paths of finite length that terminate at a specific goal location, and therefore we consider $\gamma = 1$.

The data synthesis problem of interest in this paper is described as follows. Suppose we have a dataset $\mathcal{Z} = \{\mathbf{s}^0, \mathbf{s}^1, \dots, \mathbf{s}^N\}$, of a finite number of paths traversed by an AV under some policy. We would like to synthesize another dataset $\bar{\mathcal{Z}} = \{\bar{\mathbf{s}}^0, \bar{\mathbf{s}}^1, \dots, \bar{\mathbf{s}}^K\}$, that is in some sense *similar* to \mathcal{Z} . Ideally, we want: (1) the size N of the original dataset \mathcal{Z} to be “small” and (2) low computational effort to synthesize $\bar{\mathcal{Z}}$ of a “large” size K . Similarity of \mathcal{Z} and $\bar{\mathcal{Z}}$ may be evaluated in different ways, including similarity of their statistical distributions or the closeness of data points to a common benchmark.

We consider a specific instance of this general problem that addresses minimum exposure to adverse environmental conditions during traversal to a fixed goal location \bar{x} . The environment is characterized by a *threat field* $c : \mathbb{R}^2 \times \mathbb{R}_{\geq 0} \rightarrow \mathbb{R}_{> 0}$, which is a time-varying strictly positive

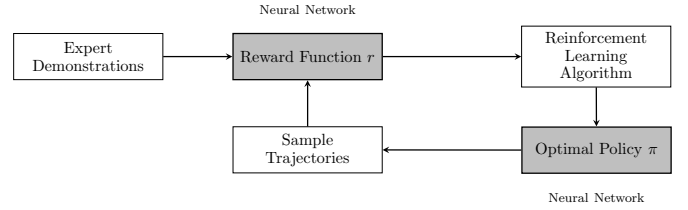


Fig. 1. Schematic illustration of IRL.

scalar field with higher intensity regions corresponding to potentially hazardous and unfavorable conditions to the AV. We are interested in policies that minimize the AV’s exposure to threat. Note that the high-level description “minimize exposure to threat” may be interpreted via several slightly different reward functions, as we discuss later in this paper.

3. METHOD

In this section, we describe the training of an IRL model using a training dataset of paths. An IRL model simultaneously learns an optimal policy, ideally $\pi^* = \arg \sup_{\pi} V^\pi$, and a reward function. To this end, recall that a reinforcement learning (RL) model learns an optimal policy for a *given* reward function. One of the standard methods of training an RL model is *Q-learning*. The *action-value function* $Q^\pi : \mathcal{S} \times \mathcal{U} \rightarrow \mathbb{R}$ maps a state-action pair to the long-term expected reward with initial state s_0 and initial action u_0 under the policy π . The optimal state-action value function is $Q^*(s, u) = \sup_{\pi} Q^\pi(s, u)$, i.e., $Q^*(s, u) \geq Q^\pi(s, u)$ for each $s \in \mathcal{S}$, each $u \in \mathcal{U}$, and for any policy π . It may be shown (Arora and Doshi, 2021) that $V^{\pi^*}(s) = \sup_{u \in \mathcal{U}} Q^*(s, u)$.

Q^* must satisfy the Bellman equation, namely,

$$Q^\pi(s, u) = r(s, u, s') + \gamma \max_{u' \in \mathcal{U}} Q^\pi(s', \pi(s')). \quad (1)$$

RL attempts to learn Q^* , after which the optimal policy π^* is defined as (Arora and Doshi, 2021; Kang et al., 2023):

$$\pi^*(s) = \arg \max_{u \in \mathcal{U}} Q^*(s, u). \quad (2)$$

To train an RL model, the rewards for all state-action-state transitions should be known. However, designing an accurate reward function may be challenging in some applications and/or an improperly designed reward function may lead to convergence to a sub-optimal policy. When the reward is unavailable, it is possible to train an IRL model that learns from data not only the optimal policy (like RL) but also the reward function simultaneously, as illustrated in Fig. 1. For an MDP $\langle \mathcal{S}, \mathcal{U}, \tau \rangle$ and a dataset \mathcal{Z} described as above, IRL attempts to learn a reward function r and a policy π^* that is optimal for the reward r , such that the errors between paths under π^* and those in the dataset are minimized (Martinez-Gil et al., 2020).

Per Martinez-Gil et al. (2020), we introduce a feature vector $\phi_s \in \mathbb{R}^{2(|\mathcal{U}|+1)}$ associated with each state that is used to formulate the reward function. Specifically:

$$\phi_s := (c(x_s, t_s), \|x_s - \bar{x}\|, c(x_{s'}, t_{s'}), \|x_{s'} - \bar{x}\|, \dots),$$

where s' indicates each neighbor of s . We assume that the reward function to be learned is a linear combination of some of the features, namely:

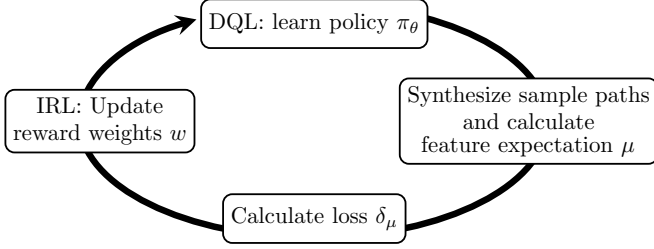


Fig. 2. Illustration of the IRL and DQL training processes.

$$r(s, u, s') := w_1 c(x_{s'}, t_{s'}) + w_2 \|x_{s'} - \bar{x}\|. \quad (3)$$

In other words, we model the reward function as a linear combination of the threat intensity and distance from the next state to the goal location.

The training process of the proposed IRL model is described in Algorithm 1, which provides the reward learning algorithm, and Algorithm 2, which describes the Q-learning algorithm. The iterative interactions of the two algorithms are illustrated in Fig. 2.

3.1 IRL and Reward Learning

The proposed IRL training algorithm iteratively updates the reward weights (w_1, w_2) based on errors between a sample set of optimal paths synthesized using the learned reward and the paths in the training dataset \mathcal{Z} of size N . To this end, we first calculate a feature expectation vector $\mu_{\mathcal{Z}} \in \mathbb{R}^2$ over the training data as follows. For each finite path $\mathbf{s}^n = (s_0^n, \dots, s_k^n, \dots, s_{L_n}^n) \in \mathcal{Z}$, we calculate an aggregate feature $\Phi_n := \sum_{k=0}^{L_n} \phi_{s_k^n}[1:2]$. The feature expectation vector is the average of Φ_n over the dataset:

$$\mu_{\mathcal{Z}} := \frac{1}{N} \sum_{n=1}^N \Phi_n = \frac{1}{N} \sum_{n=1}^N \sum_{k=0}^{L_n} \phi_{s_k^n}[1:2].$$

At the i^{th} training iteration, Algorithm 1 executes Q-learning (Algorithm 2) for M_E episodes to find an optimal policy π_{θ^i} using the reward function at the current iteration. Here, θ^i denotes the parameters of the Q-learning model at iteration i , discussed in §3.2. Using this optimal policy π_{θ^i} and a sample of initial states taken from \mathcal{S} , we find a set of K paths resulting from this policy. Each of these sample paths either terminates at the goal location or after a prespecified maximum number of transitions $M_P \in \mathbb{N}$. The magnitude of error between $\mu_{\mathcal{Z}}$ and the feature expectation vector over these paths provides an update to the reward weights w^i and the iterations continue.

Algorithm 1 is initialized with an initial guess for the reward weights, e.g., $w^0 := \mu_{\mathcal{Z}}$. The parameters θ^0 are initialized to arbitrary values. The algorithm terminates when the error reduces below a desired threshold $e_{\mu} > 0$, or returns failure to do so after a prespecified maximum number of iterations $M_I \in \mathbb{N}$. The hyperparameter η_I in Algorithm 1 is the learning rate. The numerical values of w^i and μ^i are scaled, shifted, and clipped appropriately to ensure convergence of the deep Q-learning algorithm.

3.2 Deep Q-Learning

We implement a Q-learning model as a multi-layer perceptron neural network, henceforth called the deep Q-learning

Algorithm 1 Iterative schema for IRL

```

 $i := 0;$ 
Set  $\mu^0 := w^0$  and  $\mu := (0, 0);$ 
while  $\|\mu - \mu_{\mathcal{Z}}\| \geq e_{\mu}$  and  $i \leq M_I$  do
  for  $M_E$  episodes do
     $\pi_{\theta^i} :=$  output of Deep Q-learning (Algorithm 2)
  end for
  for  $n = 1, 2, \dots, K$  do
    Sample initial state  $s_0^n$  from  $\mathcal{S};$ 
     $k := 1; \Phi_n := (0, 0);$ 
    while  $k < M_P$  do
      Find neighbor  $s_k^n$  such that
         $\tau(s_{k-1}^n, \pi_{\theta^i}(s_{k-1}^n), s_k^n) = 1;$ 
       $\Phi_n := \Phi_n + \phi_{s_k^n}[1:2];$ 
      if  $x_{s_k^n} = \bar{x}$  then
        break;
      end if
       $k := k + 1;$ 
    end while
  end for
  Calculate  $\mu := \frac{1}{K} \sum_{n=1}^K \Phi_n$  and  $\delta_{\mu} := \mu - \mu^i;$ 

   $\mu^{i+1} := \mu^i + \frac{1}{\|\delta_{\mu}\|} \langle \delta_{\mu}, \mu^i \rangle \delta_{\mu};$ 

  Update  $w^{i+1} := \eta_I \mu^{i+1} + (1 - \eta_I) w^i;$ 
   $i := i + 1;$ 
end while
return  $w := w^i$  and  $\pi^* := \pi_{\theta^i}$ 

```

(DQL). The parameters (weights and biases) in this DQL model are collectively denoted θ . The proposed DQL training process, described in Algorithm 2, is a modified form of the work by Mnih et al. (2013).

Algorithm 2 maintains parameters of the DQL model of the state-action value function, denoted Q , as well as a “mirror” model Q' . Whereas Q is the desired DQL model, maintaining Q' helps in the convergence of the training of Q . The parameters of Q' are denoted θ' . Note that the parameters of Q and Q' are initialized only once in Algorithm 1 and then maintained in memory between successive calls to Algorithm 2. Because the Q function depends on the reward function, this DQL model is parametrized by the reward weights w^i . To explicitly indicate the parameters, we denote the two DQL models by Q_{θ} and $Q'_{\theta'}$, respectively.

The parameters of $Q'_{\theta'}$ are updated either using a soft update or a hard reset, whereas the weights based on Q_{θ} . At its j^{th} training iteration, we select an action either randomly or by maximizing the currently learned Q_{θ} . This choice is based on a decreasing probabilistic threshold ε of selecting a random action (Mnih et al., 2013), which similar to the random exploration step in evolutionary optimization algorithms like simulated annealing. A soft (gradient descent-like) update of θ' occurs at each iteration, whereas a hard reset occurs whenever a mean-squared error loss reduces below a prespecified threshold $\bar{\ell}$.

Whereas the Q_{θ} and $Q'_{\theta'}$ functions map state-action pairs to a value, it is numerically convenient set up the DQL models to accept the feature vector ϕ_s as input instead

of an (s, u) pair. Note that the same input information is preserved in either case.

Algorithm 2 executes for a fixed number of iterations M_Q .

Algorithm 2 Deep Q-Learning at i^{th} IRL iteration

```

 $j := 0$ 
while  $j \leq M_Q$  do
   $\ell \equiv \emptyset$ 
  Sample  $z \sim \text{U}(0, 1)$ 
  for  $s \in \mathcal{S}$ , do
    if  $z < \varepsilon$  then
      Randomly select  $u_s^* \in \mathcal{U}$ ;
    else
      Find  $u_s^* := \arg \max_{u \in \mathcal{U}} Q_\theta(s, u; w^i)$ ;
    end if
    Find  $s'$  such that  $\tau(s, u_s^*, s') = 1$ ;
    Calculate the loss
     $\ell_s := r(s, u_s^*, s') - Q_\theta(s, u_s^*; w^i) + \gamma \max_{u_{s'}^* \in \mathcal{U}} Q_{\theta'}(s', u_{s'}^*; w^i)$ ;

    Append  $\ell_s$  to  $\ell$ 
  end for
  Update  $\theta := \arg \min_\theta \|\ell\|^2$ 
  Soft update:  $\theta' := \eta_{Q'} \theta_q + (1 - \eta_{Q'}) \theta'$ ;
   $j \leftarrow j + 1$ ;
end while
if  $\|\ell\| \leq \bar{\ell}$  then
  Hard reset:  $\theta' := \theta$ 
end if
return  $\pi_{\theta'}(s) := \arg \max_{u \in \mathcal{U}} Q_\theta(s, u; w^i)$ .

```

At the j^{th} iteration, the selection probabilistic threshold ε is chosen as

$$\varepsilon := \varepsilon_0 + (\varepsilon_1 - \varepsilon_0) \exp(-j/d),$$

where ε_0 , ε_1 , and d are hyperparameters to be tuned.

3.3 Tuning Hyperparameters

To tune the relevant hyperparameters, it is important to consider the stability of training each of the neural network models mentioned above.

In Algorithm 1, the error threshold e_μ dictates the level of accuracy for the reward function loss. In other words, it determines when the policy is sufficiently trained. The maximum number of transitions allowed in a path, M_P , determines the length of the feature function for each path. A larger value of M_P penalizes non-convergent paths more than a smaller value. Ideally, the number of points calculated according to the learned policy should be significantly larger than the maximum ideal path length. This appropriately penalizes paths that remain within the field yet do not converge and encourages the algorithm to find convergent solutions.

In Algorithm 2, the learning rates $\eta_{Q'}$ and η_Q used to update θ' and θ , respectively, should be sufficiently small that the network is able to converge. The selection threshold hyperparameters ε_1 , ε_0 , and d determine the length of random exploration to the time spent refining the current policy.

The values of various hyperparameters, tuned after several numerical experiments, are provided in Table 1.

Table 1. Tuned Values of Hyperparameters

Hyperp.	Value	Hyperp.	Value	Hyperp.	Value
M_P	500	M_E	300	M_Q	25
η_I	0.01	η_Q	0.005	$\eta_{Q'}$	0.001
ε_0	0.051	ε_1	0.95	d	500
e_μ	0.01				

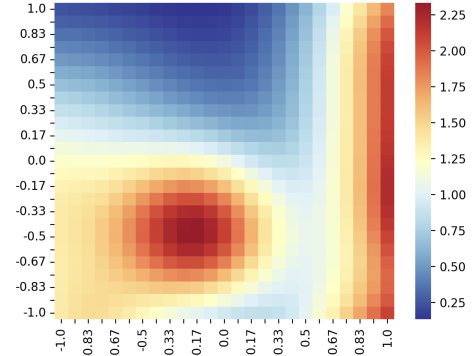


Fig. 3. Sample static threat field.

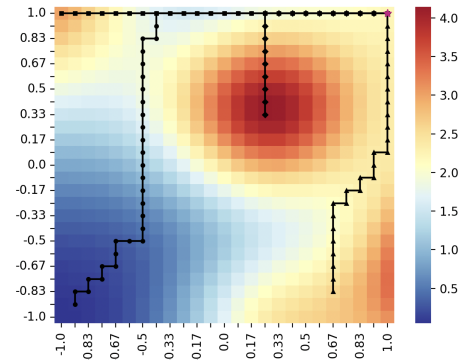


Fig. 4. Examples of minimum threat exposure paths in the training dataset \mathcal{Z} for the static case.

4. RESULTS

We perform numerical experiments with static and dynamic threat fields, as illustrated in Figs. 3 and 5. The spatial discretization is over $N_G = 625$ points in a uniform 25×25 grid, whereas temporal discretization is over $N_T = 50$ time steps. Various examples of static fields are constructed using a finite series of radial basis functions with randomly chosen coefficients. To construct evolving threat fields, as illustrated in Fig. 5, we use linear interpolation between two randomly generated static fields. The environment is restricted to a non-dimensional square region $[-1, 1] \times [-1, 1]$. The goal location is fixed at $\bar{x} = (1, 1)$.

First, we study the performance of the proposed IRL model for “pure” minimum threat exposure paths. This means, in the static case, each path $s = (s_0, s_1, \dots, s_L)$ in the dataset \mathcal{Z} satisfies $x_{s_L} = \bar{x}$ and minimizes $\sum_{k=0}^L c(x_{s_k})$ over all paths between the same start and goal locations. Figure 4 illustrates some such paths. Minimum threat exposure is similarly defined for dynamic threat fields, i.e., an expert path minimizes $\sum_{k=0}^L c(x_{s_k}, t_{s_k})$, where $t_{s_k} = t_{s_{k-1}} + \delta_t$. The training dataset is assumed to be noiseless, i.e., the paths in \mathcal{Z} are exactly optimal.

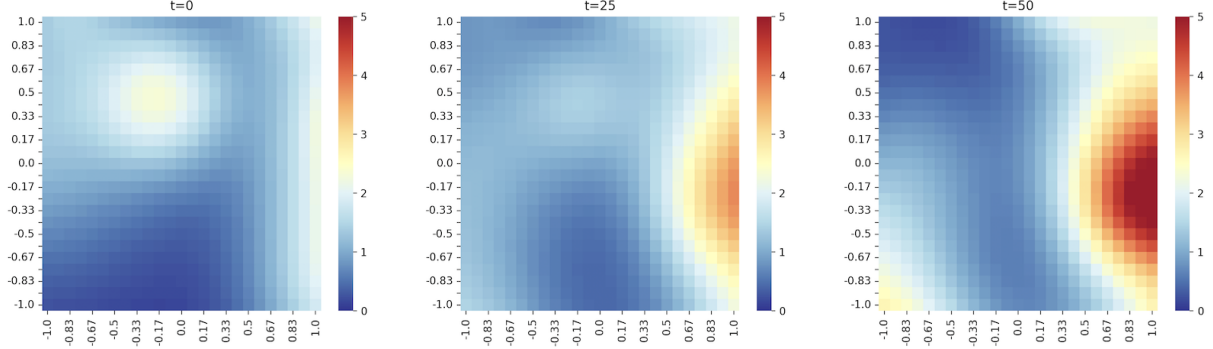


Fig. 5. Sample evolution of a dynamic threat field.

In each case, we validate our IRL algorithm by comparing the costs of paths generated by the trained policy π_θ against true optimal paths for various initial states. If a true optimal path for a particular initial state is not already provided in \mathcal{Z} , we can easily calculate it using Dijkstra’s algorithm.

The software developed for training the models reported in this paper is available: <https://github.com/aeballentine/IRL-minimum-threat-navigation.git>.

4.1 Static Threat Fields

The initial guess for the reward function weights is $w^0 = (-1, -1)$, i.e., $r(s, u, s') = -c(x_{s'}, t_{s'}) - \|x_{s'} - \bar{x}\|$, which is an intuitively reasonable guess for the reward for minimum threat exposure.

Figure 6 provides a comparison of the value functions, i.e., costs to reach the goal \bar{x} learned by the proposed IRL model (Fig. 6b) and as calculated using Dijkstra’s algorithm (Fig. 6a). Figure 6c shows the error between the two value functions. Note that the error is in general small, and the maximum error is around 15% for initial states farther away from the goal location, which indicates a good performance of the proposed IRL model.

Figure 7 gives the mean and percent error over multiple training instances, which are trained on distinct threat fields. Recall that the probabilistic threshold ε introduces inherent stochasticity in the DQL training, which may lead to different policies. Note that some policy neural networks are disregarded if the algorithm is not able to converge to the finish from all possible starting locations in the threat field. We chose to filter out these results as they result from sub-optimal training of the neural network during the Q-learning phase. Figure 7a shows that the farther away from the goal location, the worse the policy performs in general. For starting locations which are along the boundary of the graph, the IRL model is easily able to mimic the optimal path, leading to low error along the top and right borders of the threat field.

4.2 Time-Varying Threat Fields

Learning to navigate through time-varying threat fields involves the same training techniques, but requires a new definition of the transitions between locations, as movements process an agent through the threat field as well as

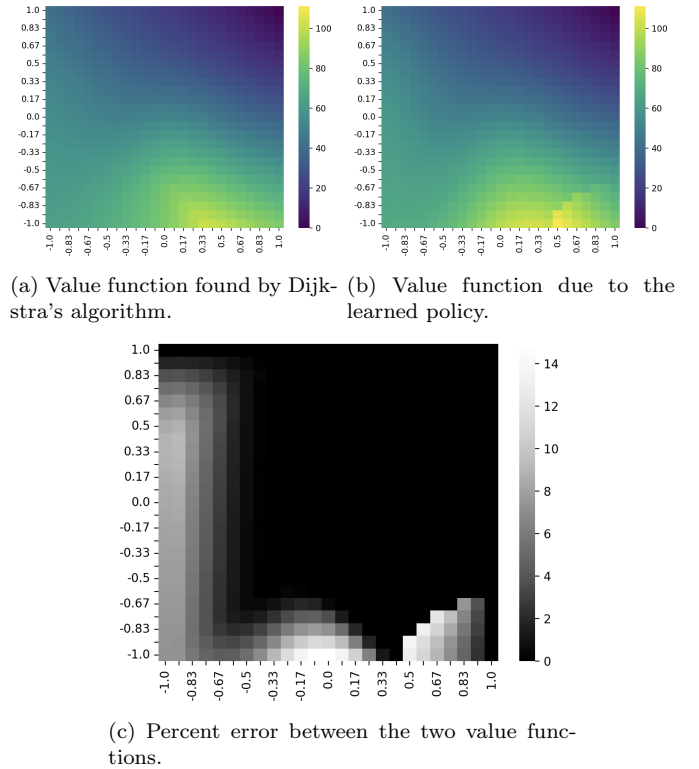


Fig. 6. Performance of the proposed IRL model for a static environment.

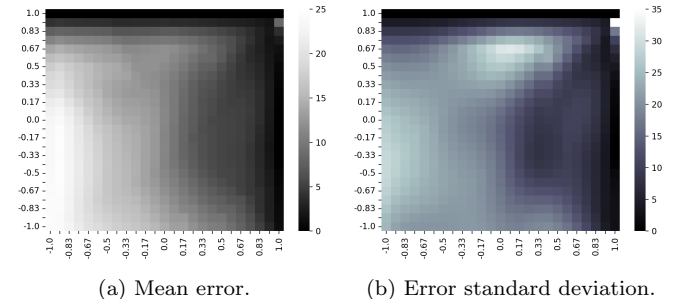


Fig. 7. Performance over 22 training instances: mean and standard deviation of percent error for the static case.

through time. We find that the inclusion of time-varying threat fields does not change the performance of the proposed IRL model. Figure 8 illustrates the performance of

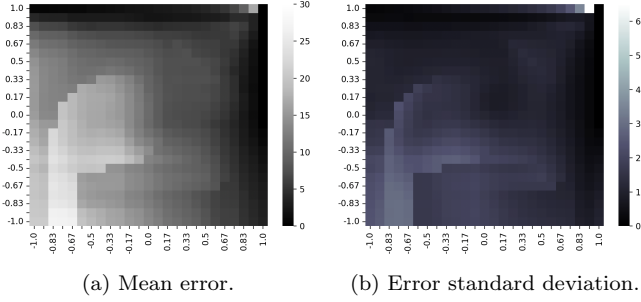


Fig. 8. Performance over 15 training instances: mean and std. dev. of percent error for the dynamic case.

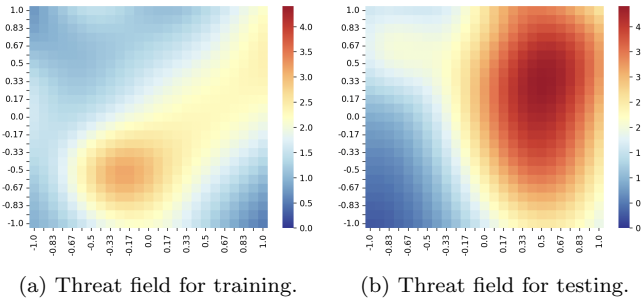


Fig. 9. Different threat fields training and testing.

15 trained policy networks by comparing the cost from each starting location to that of the optimal path.

Similar to the static case, the algorithm performs well closer to the finish point, but does not perform as well at locations which are farther away. Also similarly, the algorithm performs better, in general, along the upper and right edge, as the path to the finish is relatively straightforward and less dependent on the maximum intensity threat through the middle of the field, where there are two feasible actions that lead closer toward the goal.

4.3 Generalization to New Environments

The results in the previous two subsections consider the overall error only for one threat field, i.e., the one provided during training. Here, we consider two evaluations: that of the threat field provided during training and a new threat field that was not seen during training. As Figs. 9a and 9b illustrate, threat fields – and, consequently, optimal policies – can differ significantly.

Figure 10a shows the error between the learned and optimal value functions for the training threat field. As expected, this error is small for most initial states. Figure 10b shows the error between the learned and optimal value functions for the test threat field. The error is small in some regions, but there is a significant set of initial states where the error is large ($\sim 30\%$). The initial states where the learned policy results in high error lie in the same regions of the environment for the training and test fields. However, for the test threat field, the error has a larger magnitude and extends farther from the edge of the threat field.

In summary, we note the potential for generalization of the proposed IRL model to new threat fields unseen during

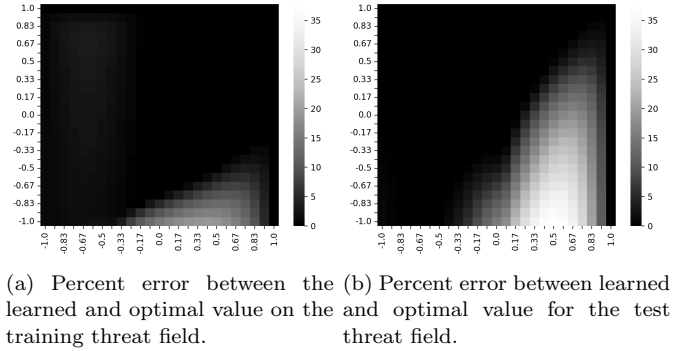


Fig. 10. Percent error for a threat field provided for training and for a different test threat field.

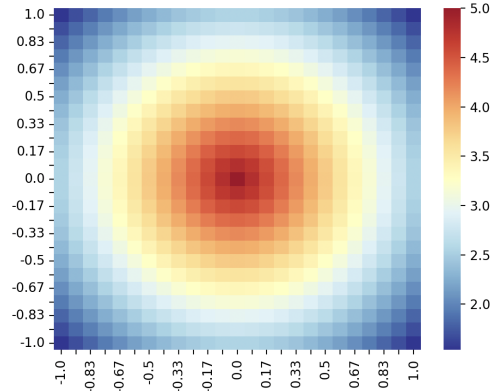


Fig. 11. Simple threat field for the purposes of training over two distinct datasets.

training, especially if a diverse set of threats is used during training.

4.4 Policy Discrimination

We return to the original motivation of performance analysis of an AV’s autonomous navigation from a limited amount of observed data. Here we focus on the problem of the ability to the proposed IRL model to synthesize data that match *different* datasets with distinct characteristics. Informally, suppose we have two different blackbox autonomy stacks that are characterized at the high level by “minimum threat exposure.” The datasets of paths resulting from each of these stacks under the same threat field are different, which implies that the exact cost function used by each stack may be slightly different. We would like to synthesize data that resembles each dataset.

To this end, we consider two datasets \mathcal{Z}_A and \mathcal{Z}_B for a static threat field shown in Fig. 11. \mathcal{Z}_A is similar to that previously described, i.e., it consists of “pure” minimum threat exposure paths.

For \mathcal{Z}_B , each path $\mathbf{s} = (s_0, s_1, \dots, s_L)$ minimizes

$$\sum_{k=0}^L c(x_{s_k}) + |x_{s_k}[2] - \bar{x}[2]|$$

over all paths between the same start and goal locations. Here $x_{s_k}[2]$ indicates the second (vertical axis) coordinate, which means that the cost function includes a $|x_{s_k}[2] - \bar{x}[2]|$ is the vertical distance between x_{s_k} and the goal location.

Informally, due to this cost function, the paths in \mathcal{Z}_B go “up and around” the high threat area in the center in Fig. 11, favoring early vertical movement towards the goal. \mathcal{Z}_A and \mathcal{Z}_B consist of $N = 500$ paths each.

We train the IRL model separately over each of these two datasets, and then synthesize $K = 624$ paths (i.e., from every possible initial location except the goal itself) from each of the learned policies. Note that we include additional entries in r and ϕ , as we split the distance component in the original feature vector into $|x_{s_k}[1] - \bar{x}[1]|$ and $|x_{s_k}[2] - \bar{x}[2]|$, i.e. into a horizontal and vertical distance between x_{s_k} and the finish. Figure 12 shows a scatter plot of the first three principal components of these synthesized outputs. The outputs of the IRL model trained on \mathcal{Z}_A are indicated in blue, whereas those trained on \mathcal{Z}_B are indicated in orange. Note that the two sets of outputs have a subset of similar paths, but also a clear distinction in outputs, as expected. These results signify that the output of the proposed IRL model is distinct for policies generated under distinct datasets, allowing us to use the output data to potentially develop more robust performance assessments or to classify new paths according to relevant policies.

5. CONCLUSIONS

In this paper we proposed an inverse reinforcement learning model to synthesize minimum threat exposure paths similar to a training dataset. We discussed details about the training process, including the IRL reward update based on errors in a feature expectation vector. The Deep Q-learning model used a probabilistic selection threshold for deciding on exploration or exploitation. Via computational studies, we considered both time-invariant (static) and time-varying (dynamic) threat fields. We found that our proposed IRL model demonstrated excellent performance in synthesizing paths from initial conditions not seen in the training dataset when the threat field matched that used for training. Furthermore, we evaluated our model’s performance on unseen threat fields and found low error. Finally, we demonstrated our model’s ability to synthesize distinct datasets when we trained it on different datasets with distinct characteristics.

ACKNOWLEDGEMENTS

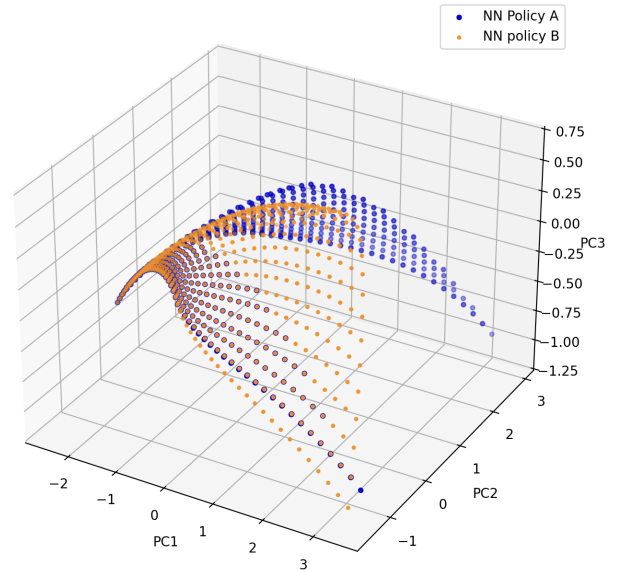
The authors are grateful to Prof. Randy Paffenroth, Mathematical Sciences Dept. and Computer Science Dept. at WPI, for his guidance and insights during the development of the proposed IRL model.

REFERENCES

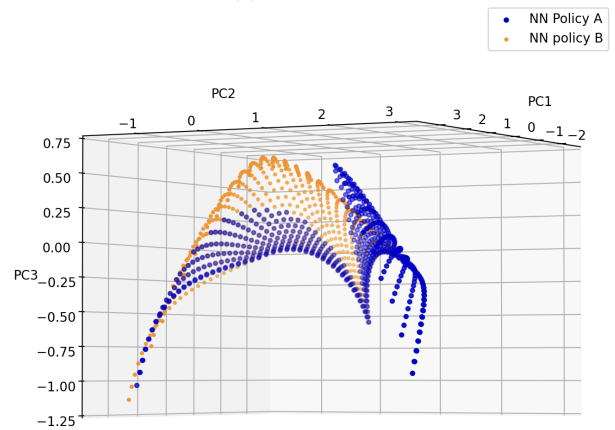
Arora, S. and Doshi, P. (2021). A survey of inverse reinforcement learning: Challenges, methods and progress. *Artificial Intelligence*, 297, 103500. doi:10.1016/j.artint.2021.103500.

Baimukashev, D., Alcan, G., and Kyrki, V. (2024). Automated Feature Selection for Inverse Reinforcement Learning. doi:10.48550/arXiv.2403.15079. URL <http://arxiv.org/abs/2403.15079>. ArXiv:2403.15079 [cs].

Brown, D.S. and Niekum, S. (2019). Machine Teaching for Inverse Reinforcement Learning: Algorithms and



(a) PCA view 1.



(b) PCA view 2.

Fig. 12. Scatter plot of first three principal components of output datasets of the proposed IRL model trained under two distinct datasets.

Applications. *Proceedings of the AAAI Conference on Artificial Intelligence*, 33(01), 7749–7758. doi:10.1609/aaai.v33i01.33017749.

Cao, H., Cohen, S., and Szpruch, L. (2021). Identifiability in inverse reinforcement learning. volume 34, 12362–12373. Curran Associates, Inc.

Dong, C. and Wang, Y. (2024). Towards Generalized Inverse Reinforcement Learning. doi:10.48550/arXiv.2402.07246. URL <http://arxiv.org/abs/2402.07246>. ArXiv:2402.07246 [cs].

Feng, Z., Xue, B., Wang, C., and Zhou, F. (2024). Safe and socially compliant robot navigation in crowds with fast-moving pedestrians via deep reinforcement learning. *Robotica*, 42(4), 1212–1230.

François-Lavet, V., Henderson, P., Islam, R., Bellemare, M.G., and Pineau, J. (2018). An Introduction to Deep Reinforcement Learning. *Foundations and Trends® in Machine Learning*, 11(3-4), 219–354. doi:10.1561/22000000071.

Huang, Z., Liu, H., Wu, J., and Lv, C. (2023). Conditional Predictive Behavior Planning with Inverse Reinforce-

- ment Learning for Human-like Autonomous Driving. doi:10.48550/arXiv.2212.08787. URL <http://arxiv.org/abs/2212.08787>. ArXiv:2212.08787 [cs].
- Kang, L., Liao, X., Liu, J., and Luo, Y. (2023). Deep estimation for Q* with minimax Bellman error minimization. *Information Sciences*, 648, 119565. doi:10.1016/j.ins.2023.119565.
- Likmeta, A., Metelli, A.M., Ramponi, G., Tirinzoni, A., Giuliani, M., and Restelli, M. (2021). Dealing with multiple experts and non-stationarity in inverse reinforcement learning: an application to real-life problems. *Machine Learning*, 110(9), 2541–2576. doi:10.1007/s10994-020-05939-8.
- Martinez-Gil, F., Lozano, M., García-Fernández, I., Romero, P., Serra, D., and Sebastián, R. (2020). Using Inverse Reinforcement Learning with Real Trajectories to Get More Trustworthy Pedestrian Simulations. *Mathematics*, 8(9), 1479. doi:10.3390/math8091479.
- Mnih, V., Kavukcuoglu, K., Silver, D., Graves, A., Antonoglou, I., Wierstra, D., and Riedmiller, M. (2013). Playing Atari with Deep Reinforcement Learning. URL <http://arxiv.org/abs/1312.5602>. ArXiv:1312.5602 [cs].
- Naranjo-Campos, F.J., Victores, J.G., and Balaguer, C. (2024). Expert-Trajectory-Based Features for Apprenticeship Learning via Inverse Reinforcement Learning for Robotic Manipulation. *Applied Sciences*, 14(23), 11131. doi:10.3390/app142311131.
- Ng, A.Y. and Russell, S.J. (2000). Algorithms for Inverse Reinforcement Learning. In *Proceedings of the Seventeenth International Conference on Machine Learning*, ICML '00, 663–670. Morgan Kaufmann Publishers Inc., San Francisco, CA, USA.
- Ruthotto, L. and Haber, E. (2021). An introduction to deep generative modeling. *GAMM-Mitteilungen*, 44(2), e202100008. doi:<https://doi.org/10.1002/gamm.202100008>.
- Tucker, A., Gleave, A., and Russell, S. (2018). Inverse reinforcement learning for video games. URL <http://arxiv.org/abs/1810.10593>. ArXiv:1810.10593 [cs].
- Young, S.H., Mazzuchi, T.A., and Sarkani, S. (2017). A framework for predicting future system performance in autonomous unmanned ground vehicles. *IEEE Transactions on Systems, Man, and Cybernetics: Systems*, 47(7), 1192–1206. doi:10.1109/TSMC.2016.2563403.
- Zare, M., Kebria, P.M., Khosravi, A., and Nahavandi, S. (2024). A Survey of Imitation Learning: Algorithms, Recent Developments, and Challenges. *IEEE Transactions on Cybernetics*, 54(12), 7173–7186. doi:10.1109/TCYB.2024.3395626.
- Ziebart, B.D., Maas, A., Bagnell, J.A., and Dey, A.K. (2008). Maximum entropy inverse reinforcement learning. In *Proceedings of the 23rd National Conference on Artificial Intelligence - Volume 3, AAAI'08*, 1433–1438. AAAI Press. Place: Chicago, Illinois.